Optik 125 (2014) 1667–1670

Contents lists available at ScienceDirect

Optik

journal homepage: www.elsevier.de/ijleo

# Verification of surface WGM in radio frequency band

Jie Yang[a], Jingjing Yang[a], Ming Huang[a,*], X.Z. Dai[b], Mohai Guo[a]

[a] Wireless Innovation Lab, School of Information Science and Engineering, Yunnan University, Kunming 650091, PR China
[b] Yunnan Copper Group Co., Ltd., Kunming 650051, PR China

ARTICLE INFO

*Article history:*
Received 23 April 2013
Accepted 5 September 2013

*Keywords:*
SWGM sensor
Metamaterials
LC network

ABSTRACT

The ideas of generating surface whispering gallery mode (SWGM) through coating a microresonator with a layer of metamaterials is proposed in our previous work. In this paper, we verify the SWGM with a square resonator based on two-dimensional LC network in radio frequency band. The equivalent node voltage distribution matrix of this resonator is derived. Results show that node voltage can be amplified when the square resonator is covered with a layer of double negative metamaterials. The performance of the metamaterial resonator as a dielectric sensor with excellent sensitivity has been demonstrated. This work may put a great step toward the realization of SWGM sensors using metamaterials.


## 1. Introduction

In the past few years, optical microresonators which support whispering gallery modes (WGMs) have attracted increasing interest [1–5]. One of the most important requirements for WGM resonators is a high refractive index contrast between the cavity and the surrounding media. For this reason, a quasi-freestanding resonator embedded in air is the preferred solution [6]. The WGM microresonators have been widely used in sensor technology for the detection of single molecules [7,8], nanoparticles [9,10], counterfeit drug [11], and the measurement of temperature [12], etc. However, energies of WGM are confined within the dielectric resonator, and evanescent wave in the surrounding media is rather weak, which restrict the improvement of sensitivity.

In 2000, Pendry [13] demonstrated the "perfect lens" concept by showing theoretically that the evanescent waves from an image can be amplified by negative refractive index slab. After that, perfect imaging becomes a research hot spot [14,15]. The perfect lens effect was demonstrated experimentally by Fang et al. [16] in 2005 using silver slabs. It has been found that for a metamaterial slab with thickness of d and dielectric loss of $\delta$, the resolution will be $\Delta = 2\pi d/\ln(2/\delta)$ [17]. Based on the evanescent wave amplification effect of metamaterials, sensors with superior resolution have been proposed. For example, Qing et al. [18] found that metamaterials can enhance the intensity of the evanescent waves in the cladding without altering the propagation constant of the waveguide for both TE and TM modes. Taya et al. [19] investigated the metamaterial assisted slab waveguide, and they show that through inserting a layer of metamaterials with negative permittivity and negative permeability between the cladding and the guiding layer, the sensitivity can be dramatically enhanced. The nonlinear planar optical waveguide sensor with metamaterial layer is proposed by our group [20,21], and both the TE and TM mode dispersion equations are derived and analyzed in detail. The results reveal that metamaterials combined with nonlinear waveguide will further enhance the sensitivity of the optical planar waveguide sensors.

Recently, we found that when a layer of metamaterials with negative permittivity or permeability is coated on the surface of a microresonator, a new kind of resonant mode, that is, the surface whispering gallery mode (SWGM) [22] will be generated. Due to the evanescent field is amplified and penetrate into the surrounding media, sensors based on SWGM possess much higher sensitivity than traditional microresonators. In this paper, we design a SWGM resonator using transmission line metamaterials [23] based on a 2D LC network. Its performance as a dielectric sensor is analyzed in detail.

## 2. Method and simulation model

The schematic structures of the simulation model are illustrated in Fig. 1. The left and right panels of Fig. 1(a) correspond to the equivalent LC network cells of the double positive material (DPM) and the double negative material (DNM) regions. Effective permittivity and permeability of these cells are expressed as $\varepsilon_R$, $\mu_R$ and $\varepsilon_L$, $\mu_L$, respectively. The whole computational domain contains $33 \times 33$ cells, as shown in Fig. 1(b), where the black and white circles represent DNM and DPM regions, the gray circles represent the straight waveguide and the resonant ring, of which the relative permittivity is $\varepsilon_N$. The DNM layer is supposed to be deposited on the inner surface of the ring. Relative

* Corresponding author. Tel.: +86 871 5033743; fax: +86 871 5033743.
*E-mail address:* huangming@ynu.edu.cn (M. Huang).

0030-4026/$ – see front matter © 2013 Elsevier GmbH. All rights reserved.
http://dx.doi.org/10.1016/j.ijleo.2013.09.047

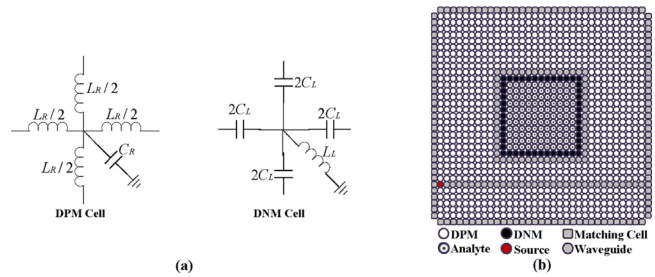


**Fig. 1.** Schematic structures of the simulation model. (a) Unit cells; (b) computational domain of the SWGM resonator.

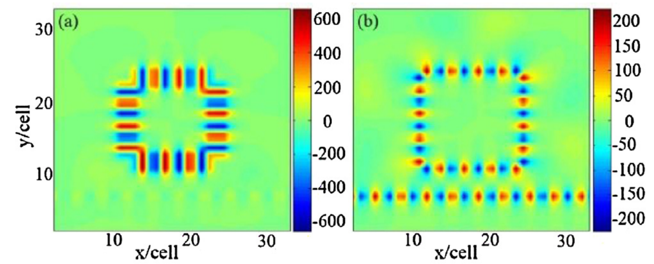


**Fig. 2.** Voltage distribution in the computational domain of the resonator. (a) With metamaterials; (b) without metamaterials.

permittivity of the analytes filling in the inner region is denoted as $\varepsilon_C$. The computational domain is surrounded by Bloch impedances which simulate the matching boundary conditions. In our design, $\varepsilon_R = \varepsilon_0$, $\mu_R = \mu_0$, $\varepsilon_L = -\varepsilon_0$, $\mu_L = -\mu_0$. The corresponding parameters of the equivalent circuit are expressed as [24]: $L_R = \mu_0 \Delta$, $C_R = \varepsilon_0 \Delta$, $L_L = 1(C_R\omega^2)$, $C_L = 1/(L_R\omega^2)$, where, $\Delta = 0.1C_0/f$, $\omega = 2\tau f$, $\Delta$ represents the dimension of the unit cell, $f$ refers to the resonant frequency of the device, and $C_0$ is the propagation velocity of electromagnetic wave in the air. For the analytes, equivalent circuit parameters satisfies $L_R = \mu_0 \Delta$, $C_R = \varepsilon_c \varepsilon_0 \Delta$.

For convenience, we mark the voltage of each grid node as $V_{x,y}$, where the subscript $x$, $y$ are used to describe the position of node, i.e., the coordinates of the nodes in horizontal and vertical direction. Here we set the first left bottom node of the network as the origin of the coordinates, which is marked as $V_{0,0}$. According to Kirchhoff's current law and Ohm's law, the node equation is described as:

$$\frac{V_{0,0} - V_{0,1}}{2Z_R} + \frac{V_{0,0} - V_{1,0}}{2Z_R} + \frac{2V_{0,0}}{Z_B + Z_R} + Y_R V_{0,0} = 0 \tag{1}$$

where $Z_R$, $Y_R$ and $z_B$ denote the series impedance between adjacent nodes, the parallel admittance between the node and the ground, and the Bloch impedance at the outer boundary, respectively. They can be derived as:

$$Z_R = \frac{j\omega L_R}{2}, \quad Y_R = j\omega C_R, \quad Z_B = \sqrt{\frac{\mu_R}{\varepsilon_R}},$$

Similarly, we can get all equations for the rest of nodes using the same method. After some algebraic operations, the matrix form of voltage equations can be obtained as follows:

$$\boldsymbol{KV} = \boldsymbol{C}, \tag{2}$$

where $\boldsymbol{K}$ is the coefficient matrix derived from KCL equations, $\boldsymbol{V}$ is the matrix constituted by node voltages, and $\boldsymbol{C}$ is a constant matrix whose element values are determined by the position of the excitation source. The matrix $\boldsymbol{K}$ is expressed as:

$$\boldsymbol{K} = \begin{bmatrix} P_L & 0 & 0 \\ 0 & N & 0 \\ 0 & 0 & P_R \end{bmatrix} \tag{3}$$

$\boldsymbol{K}$ is composed of 9 square matrixes, including $\boldsymbol{P}_L$, $\boldsymbol{P}_R$, $\boldsymbol{N}$, and 6 zero matrixes. The expressions of matrixes, $\boldsymbol{P}_L$, $\boldsymbol{P}_R$, $\boldsymbol{N}$ and their element values can be obtained according to the mentioned proposed in Ref. [25]. $\boldsymbol{V}$ and $\boldsymbol{C}$ are both matrixes in the size of $33^2 \times 1$ as shown in Eqs. (4) and (5). By solving the above matrix equation, the node voltages can be obtained.

$$\boldsymbol{V} = \begin{bmatrix} V_{0,0} & \cdots & V_{0,32} & V_{1,0} & \cdots & V_{1,32} & \cdots & V_{32,0} & \cdots & V_{32,32} \end{bmatrix}^T \tag{4}$$

$$\boldsymbol{C} = \begin{bmatrix} C_{0,0} & \cdots & C_{0,32} & C_{1,0} & \cdots & C_{1,32} & \cdots & C_{32,0} & \cdots & C_{32,32} \end{bmatrix}^T \tag{5}$$

## 3. Numerical simulations and discussions

In order to analyze the electromagnetic properties of the SWGM as shown in Fig. 1, we assume that the excitation source is a current source with frequency of $f = 522.5$ MHz, values of the inductors, capacitors, and Bloch impedances are: $L_R = 72$ Nh, $C_R = 0.5$ pF, $L_L = 182.51 =$ nH, $C_L = 2.5719$ pF, $Z_B = 377\ \Omega$, the high refractive index materials are $SiO_2$, i.e., $\varepsilon_N = 3.2^2 = 10.24$, here, the inner region is supposed to be air with $\varepsilon_c = 1$. In the simulation, the current source with amplitude of 1 A is connected between node (0, 5), i.e., the center of the first cell of the straight waveguide and the ground to generate a point source excitation. Therefore, the value of element $C_{0.5}$ in constant matrix $C$ becomes $2Z_R$, and the other values are zero. Substitute the above parameters into the node voltage matrix Eq. (2), and the equivalent voltage distribution of computational domain at the resonant state of $f = 528.22$ MHz is obtained, as shown in Fig. 2(a). As a comparison, the voltage distribution of the computational domain where the DNM ring is replaced by DPM is plotted in Fig. 2(b). The resonant frequency is $f = 522.62$ MHz. We can observe that voltage distribution of WGM resonator is confined within the ring, and the penetration of evanescent wave is rather weak. But when SWGM is excited, evanescent wave can be amplified, and penetrates deep into the surrounding media. Meanwhile, we have simulated the performance of the device using the commercial software ADS (Advanced Design System). The results agree well with Fig. 2, which further confirms the effectiveness of the proposed method.

To give a vivid picture of the field amplification characteristics, we plot the voltage distribution along the center line of the simulation model, as shown in Fig. 3. It is seen that the maximum voltage amplitude in the case of metamaterial resonator is three times higher than the resonator without the metamaterial layer.

To investigate the sensitivity of the metamaterial resonator, we suppose that a slight change ($\Delta\varepsilon_c$) is introduced into the permittivity of the analytes: $\varepsilon'_c = \varepsilon_c + \Delta\varepsilon_c$. When $\Delta\varepsilon_c$ increases from 0 to 1 with an interval of 0.1, the variations of relative frequency shift ($\Delta f$) for both the homogeneous sensing and surface sensing are simulated, as shown in panels (a) and (b) of Fig. 4. In the simulation, the resonant frequency ($f_i$) for each minor change of analysts' permittivity is recorded. Relative frequency shift is calculated as $\Delta f = f_i - f_1$. Here, $f_1$ is the resonant frequency for $\varepsilon'\varepsilon'_c = 1$. In the case of homogeneous sensing, we assume that the analytes fill in the whole inner region of the resonator. For surface sensing, the first layer of the components in the inner region that adhere to the metamaterials is supposed to be the analytes. As a comparison, simulation results of the resonator without the metamaterial